Isotopic and Compositional Variations in Single Nuclear Fuel Pellet Particles Analyzed by Nanoscale Secondary Ion Mass Spectrometry

Fallon, Connaugh M.

2020-01-14

Fallon , C M , Bower , W R , Lyon , I C , Livens , F R , Thompson , P , Higginson , M , Collins , J , Heath , S L & Law , G T W 2020 , ' Isotopic and Compositional Variations in Single Nuclear Fuel Pellet Particles Analyzed by Nanoscale Secondary Ion Mass Spectrometry ' , ACS Omega , vol. 5 , no. 1 , pp. 296-303 . https://doi.org/10.1021/acsomega.9b02703

http://hdl.handle.net/10138/309573
https://doi.org/10.1021/acsomega.9b02703

other
publishedVersion

ACS OMEGA

Article

Cite This: ACS Omega 2020, 5, 296−303

http://pubs.acs.org/journal/acsodf

Isotopic and Compositional Variations in Single Nuclear Fuel Pellet Particles Analyzed by Nanoscale Secondary Ion Mass Spectrometry

Connaugh M. Fallon,*[,†,‡] William R. Bower,[†,∥] Ian C. Lyon,[‡,§] Francis R. Livens,[†,‡] Paul Thompson,[⊥] Matthew Higginson,[⊥] Jane Collins,[⊥] Sarah L. Heath,[‡] and Gareth T. W. Law*[,‡,∥]

[†]Centre for Radiochemistry Research, Department of Chemistry, [‡]Department of Earth and Environmental Sciences and [§]Photon Science Institute, School of Natural Sciences, The University of Manchester, Manchester M13 9PL, United Kingdom

[∥]Radiochemistry Unit, Department of Chemistry, The University of Helsinki, Helsinki 00014, Finland

[⊥]Atomic Weapons Establishment, Aldermaston RG7 4PR, United Kingdom

Supporting Information

ABSTRACT: The Collaborative Materials Exercise (CMX) is organized by the Nuclear Forensics International Technical Working Group, with the aim of advancing the analytical capabilities of the participating organizations and providing feedback on the best approaches to a nuclear forensic investigation. Here, model nuclear fuel materials from the 5th CMX iteration were analyzed using a NanoSIMS 50L (CAMECA) in order to examine inhomogeneities in the $^{235}U/^{238}U$ ratio and trace element abundance within individual, micrometer scale particles. Two fuel pellets were manufactured for the exercise and labelled CMX-5A and CMX-5B. These pellets were created using different processing techniques, but both had a target enrichment value of $^{235}U/^{238}U = 0.01$. Particles from these pellets were isolated for isotopic and trace element analysis. Fifteen CMX-5A particles and 20 CMX-5B particles were analyzed, with both sample types displaying inhomogeneities in the U isotopic composition at a sub-micrometer scale within individual particles. Typical particle diameters were ∼1.5 to 41 μm for CMX-5A and ∼1 to 61 μm for CMX-5B. The CMX-5A particles were shown to be more isotopically homogeneous, with a mean $^{235}U/^{238}U$ atom ratio of 0.0130 ± 0.0066. The CMX-5B particles showed a predominantly depleted mean $^{235}U/^{238}U$ atom ratio of 0.0063 ± 0.0094, which is significantly different to the target enrichment value of the pellet and highlights the potential variation of $^{235}U/^{238}U$ in U fuel pellets at the micrometer scale. This study details the successful application of the NanoSIMS 50L in a mock nuclear forensic investigation by optimizing high-resolution imaging for uranium isotopics.

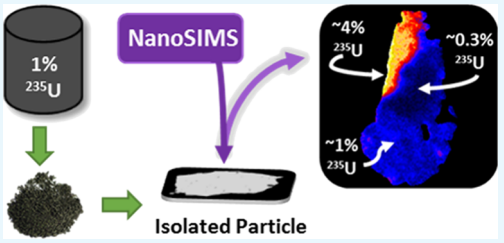

1. INTRODUCTION

Nuclear forensic science focuses on the analysis of nuclear and/or radioactive materials found outside of regulatory control.[1,2] By characterizing the chemical and isotopic signatures of a sample, inferences about the material's source, processing history, and intended use can be drawn. Such information is often vital in the context of nuclear security and law enforcement investigations.[2−4]

Radioactive particles are an invaluable resource for nuclear forensic investigations as fine particulates and dusts are typically present following the handling of radioactive or nuclear materials.[5] Particulate fragments of source materials can yield valuable isotopic and chemical information on the sub-micrometer scale, thereby providing a characteristic "fingerprint" of the parent material.[6] Furthermore, particulates can also provide a mechanistic insight into their release and formation conditions following nuclear accidents, information that is vital for site remediation/decommissioning strategies and damage assessments.[6] However, the analysis of such particles can often be extremely challenging, especially given their size, limited volume, complex isotopic and elemental composition, and multiple phase distributions.[7,8] Indeed, elucidating chemical heterogeneities/homogeneities over a range of scales is a valuable characterization tool for samples of limited quantities. The development of an analytical toolkit capable of examining the microstructural, isotopic, and elemental composition of individual particles is therefore essential for advanced nuclear forensic investigations.[2,9]

Mass spectrometry is a fundamental technique in nuclear forensics, allowing for the determination of elemental, molecular, and isotopic information across a diverse range of materials.[10] Secondary ion mass spectrometry (SIMS) has already proven to be successful for single particle investigations, with specific applications in the characterization of micrometer-sized, uranium (U)-bearing samples with high spatial resolution and high mass resolution.[1,11−13] The CAMECA NanoSIMS 50L offers the high mass resolution and sensitivity of other SIMS methods, with a unique primary ion beam configuration that allows for high-spatial-resolution analysis. Indeed, a lateral resolution of ∼50 nm is achievable for both negative and positive

Received: August 21, 2019
Accepted: October 23, 2019
Published: December 27, 2019

DOI: 10.1021/acsomega.9b02703
ACS Omega 2020, 5, 296−303

secondary ions (using Cs^+ or Hyperion primary ion beam).[14] This increased spatial resolution allows for the detailed analysis of individual microparticles, revealing subtle differences in isotopic ratios and elemental composition at the nanometer scale.[15] This is particularly useful for nuclear forensic investigations where the scale of analysis can be a crucial factor in determining the enrichment and processing history of a material used as evidence for origin assessment.[9,16] Prior to the development of nanoscale SIMS (NanoSIMS) techniques, "bulk" isotopic ratios (those determined via conventional SIMS or radiochemical analyses) were typically expressed as an average for an individual microparticle (or number of particles). Indeed, conventional SIMS techniques provide a lateral resolution of several micrometers, meaning submicrometer variations in isotopic or chemical composition within individual particles cannot usually be observed.[17] As such, vital information on a material's processing history and origin can often be lost with bulk-scale analysis techniques. Thus, NanoSIMS is emerging as a vital technique in nuclear forensics, with the capability of discerning variations in isotopic content at the micrometer scale.[15]

The Nuclear Forensics International Technical Working Group (ITWG) Collaborative Materials Exercises (CMXs) have been running since 1999, with the fifth exercise (CMX-5) commencing in 2015/2016.[18] The purpose of these exercises is to simulate the real-life discovery and subsequent investigation of a nuclear material of unknown origin, using materials representative of those under regulatory control (i.e., uranium and plutonium oxides/metals).[19] The exercises provide a platform for determining the best practices for nuclear forensic laboratories while also allowing for the assessment of new experimental techniques. For U-bearing particles, ^{235}U enrichment is used as an indicator in determining anthropogenic processing and the fissile content of a material (and thereby its intended use) as natural U contains ^{234}U, ^{235}U, and ^{238}U in relative atomic abundances of 0.005, 0.72, and 99.27%, respectively.

For the CMX-5 exercise, which concluded in 2017, the participating institutions were each sent two low-enriched UO_2 fuel pellets, a specification sheet for a third theoretical fuel pellet, and a fictional description of the "find". The two fuel pellets, labelled CMX-5A and CMX-5B, were produced by the French Alternative Energies and Atomic Energy Commission (CEA, Cadarache, France), using identical feedstock mixtures of depleted uranium (DU) (UO_2, ^{235}U = 0.3 atom %) and low-enriched uranium (LEU) (UO_2, ^{235}U = 4.3 atom %) to give a final target enrichment value of $^{235}U/^{238}U$ = 0.01.[20] Although the same feedstocks were used, different sintering techniques and compaction pressures were employed for the two pellet types, resulting in a very different macrostructure between them.[20] The method used to create the CMX-5A pellet is representative of AREVA's manufacturing process for PWR fuel, termed the "normal double cycle" route.[20,21] Here, source materials are combined before undergoing a series of grinding/compaction steps. This route has an initial low-pressure compaction (50 MPa) followed by a high-pressure formatting compaction (450 MPa).[20] CMX-5B was created using the "inverse double cycle" method where a dense fuel mixture is achieved by applying a high pressure to the source materials followed by crushing/sieving and then a second low-pressure compaction.[20] This method was developed in order to create large, stable pores in the fuel material as a means of preventing fuel densification upon irradiation.[22]

Here, swipe samples containing micrometer-sized particles from the two fuel pellets (CMX-5A and CMX-5B) were analyzed using a NanoSIMS 50L in order to investigate the spatial distribution of isotopic and trace element signatures within individual particles and relate the findings to the material's provenance and processing history. It was hypothesized that the NanoSIMS 50L could be employed to understand the differences in the manufacturing processes used for the two CMX-5 fuel pellets, with wider applicability in the field of nuclear forensic science and particulate characterization. This research also provides a useful comparison to other techniques used in CMX-5, especially other SIMS techniques optimized for high-precision isotopic analysis. Using NanoSIMS, inhomogeneities in U isotopics were identified in individual particles from the CMX-5A and CMX-5B pellets, giving forensic insight into the starting materials used in their production.

2. RESULTS AND DISCUSSION

2.1. Scanning Electron Microscopy–Energy-Dispersive X-ray Spectroscopy. Several CMX-5A and CMX-5B particles were analyzed with scanning electron microscopy–energy-dispersive X-ray spectroscopy (SEM–EDX) to give a semiquantitative elemental composition. Both CMX-5A and CMX-5B displayed similar elemental profiles, with U being the major component (Figures S1 and S2). Minor trace elements (Al, Si, and Na) were also detected in both 5A and 5B particles. EDX spectra and associated images are presented in the Supporting Information, section 1.

Alumina was added to both the CMX-5A and CMX-5B pellets during fabrication; however, for CMX-5B, this additive was only introduced to the DU fraction, which was later combined with the LEU source in a soft mix.[20] Here, EDX imaging showed that Al was homogeneously dispersed throughout several particles from both the CMX-5A and CMX-5B swipes. Several particles from both samples also contained spherical Al inclusions, co-located with an increased O signal and a decreased U signal (Figure S3). However, no discernible differences were evident in the Al content of the two pellet types based on EDX analysis. One CMX-5A particle exhibited a more varied elemental profile, containing trace amounts of Na, Mg, Al, Si, S, Ca, Cr, Fe, and Cu; however, this was the only particle that exhibited such heterogeneity (Figure S1).

Particles of CMX-5A and CMX-5B displayed comparable morphologies, containing small spherical pores (<500 nm) and some larger voids (>1 μm). The frequency of pores per unit area was investigated using a subset of 13 CMX-5A and 13 CMX-5B particles. The CMX-5A particles appeared to be more porous than the CMX-5B materials, giving an average of 0.162 ± 0.091 and 0.109 ± 0.097 pores/μm^2, respectively. The measurements for the particles are given in more detail in the Supporting Information (section 2, Table S1).

2.2. NanoSIMS Imaging. *2.2.1. Uranium Isotope Calibrations.* Isotopic ratio analysis employed a combination of $^{235}U/^{238}U$, $^{235}U^{16}O/^{238}U^{16}O$, and $^{235}U^{16}O_2/^{238}U^{16}O_2$ species. A particle surface average (PSA) is presented for each CMX particle analyzed, denoting the mean isotopic ratio from the surficial layers sputtered by the NanoSIMS beam. PSAs were calculated by applying a 25% threshold to the $^{238}U^+$ secondary ion image intensity to remove the background signal, thereby creating a region of interest (ROI) around each particle. The PSA does not represent the "whole" particle average as this would require complete destructive sputtering of each particle.

DOI: 10.1021/acsomega.9b02703
ACS Omega 2020, 5, 296–303

Table 1. True U Ratio Values for CRM U630[25] and Natural Uranophane, with the Measured PSA Isotopic Ratios for the U^+, UO^+, and UO_2^+ Species Acquired with the NanoSIMS 50L

			measured values		
calibration material	isotopic ratio	true values[a]	U^+	UO^+	UO_2^+
CRM U630	$^{238}U/^{235}U$	5.54×10^{-1} ($\pm$ 4.9×10^{-4})		5.47×10^{-1} ($\pm$ 1.60×10^{-3})	5.52×10^{-1} ($\pm$ 1.91×10^{-3})
	$^{234}U/^{235}U$	9.77×10^{-3} ($\pm$ 6.2 10^{-6})			1.03×10^{-2} ($\pm$ 1.83×10^{-4})
uranophane	$^{235}U/^{238}U$	7.25×10^{-3}	7.49×10^{-3} ($\pm$ 1.73×10^{-5})	7.46×10^{-3} ($\pm$ 3.42×10^{-5})	7.47×10^{-3} ($\pm$ 4.39×10^{-6})
	$^{234}U/^{238}U$	5.47×10^{-5}	5.43×10^{-5} ($\pm$ 3.84×10^{-6})		5.40×10^{-5} ($\pm$ 1.67×10^{-7})

[a]Errors for the true isotopic ratios of the CRM U630 are expressed as expanded uncertainty at a 95% confidence interval. The uncertainty in the measured values is based on Poisson counting statistics.

This averaging was also applied for the assessment of the isotopic calibration materials.

Repeat analyses of the isotopic ratios were acquired to determine whether there were any variations when measuring the $^{235}U/^{238}U$, $^{235}UO/^{238}UO$, or $^{235}UO_2/^{238}UO_2$. The measurement of oxide species to determine atom ratios is a common method in NanoSIMS analysis as the oxide is cancelled out when ratioing the secondary ion images.[23] The UO^+ and UO_2^+ secondary ion species were chosen because they provided a significant increase in the secondary ion signal yield relative to U^+. This improvement in counting statistics yielded higher-resolution images, particularly for the low abundance U isotopes (^{234}U and ^{235}U). Images obtained from these repeats showed that the U^+, UO^+, and UO_2^+ signals exhibited the same spatial distribution within the particles and that ratio values for the different species are in good agreement, as shown by the PSA values in Table 1. For the purposes of this study, the UO and UO_2^+ species are assumed to accurately represent the $^{234/235}U/^{238}U$ atomic ratios. As such, the ratios of all species are expressed as the atomic values ($^{234}U/^{238}U$ and $^{235}U/^{238}U$) throughout this study, unless otherwise specified.

The $^{234}U/^{238}U$ and $^{234}UO_2/^{238}UO_2$ species were measured for several particles, but the $^{234}UO^+$ signal was not used due to an isobaric interference of $^{238}U^{12}C^+$ with $^{234}U^{16}O^+$. For $^{234}UO_2/^{238}UO_2$, the $^{238}U^{12}C^+$ content was also examined but this either gave counts below background or did not correlate spatially with the bulk U signal; thus, the probability of forming $^{238}U^{12}C^{16}O^+$ compared to $^{234}U^{16}O_2^+$ was found to be very low and did not represent a significant interference. An unresolvable mass interference is expected between the $^{235}U^+$ and $^{234}U^1H^+$ species. However, hydride contributions are typically lower than the atomic signal during SIMS analysis, and $^{234}U^1H^+$ interferences are expected to contribute less than 0.01% to the $^{235}U^+$ signal.[24] Here, $^{238}U^1H^+$ was measured from the mass spectrum of a CMX-5A particle and was shown to equal ~0.55% of the $^{238}U^+$ signal, which would equate to <1 count for the $^{234}U^1H^+$, or <0.01% of the $^{235}U^+$ signal. Thus, the $^{234}U^1H^+$ interference was deemed to be negligible for this study (see the Supporting Information, section 3, Figure S4).

The measured ratios and their certified values for the calibration materials are provided in Table 1. The statistical errors for the calibrants were low (<0.3%), but there were some systematic differences from the true values, likely resulting from instrumental fractionation. However, these differences amounted to <3% in the measured ratio and therefore have no bearing on the isotopic ratio values determined for the CMX samples. High-resolution imaging reduces the count rate for secondary ion images that can impact the precision of isotopic ratio values. Thus, the NanoSIMS 50L is complementary to other techniques that have a low spatial resolution but are optimized for high-precision isotopic analysis, such as large-geometry SIMS (LG-SIMS).

2.3. Trends in Uranium Isotopic Ratios. A total of 35 particles were analyzed by NanoSIMS: 15 from CMX-5A and 20 from CMX-5B, yielding mean $^{235}U/^{238}U$ atom ratios (summed from PSAs) of 0.0130 ($\pm$ 0.0066) and 0.0063 ($\pm$ 0.0094), respectively. An overview of the $^{235}U/^{238}U$ PSAs for each particle analyzed is presented in Figure 1. This gives a more direct

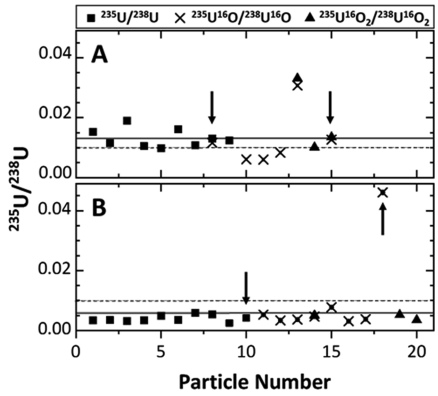

Figure 1. PSA $^{235}U/^{238}U$ isotopic ratios for the (A) CMX-5A and (B) CMX-5B particles. The isotopic species measured is indicated by symbols where the solid box is $^{235}U/^{238}U$, the cross is $^{235}U^{16}O/^{238}U^{16}O$, and the solid triangle is $^{235}U^{16}O_2/^{238}U^{16}O_2$. Mean ratios for each subset of particles are indicated by the solid line. The manufacturer target enrichment value (1% ^{235}U) is shown by the dashed line. Errors are contained within the data points. The arrows indicate the particles that have been presented in Figures 2–5. Particle numbers were assigned based on the analysis order.

comparison with the isotopic data provided by the manufacturers and the other participating laboratories in the CMX-5 exercise. However, it should be noted that NanoSIMS is a surface probe technique, and the data presented here is not from the destructive sputtering of the whole particle. Particle sizes ranged in diameter from ~1.5 to 41 μm for CMX-5A and from ~1 to 61 μm for CMX-5B, and no correlation between particle size and enrichment was identified.

The CEA has provided definitive enrichment values for the pellets of 1.0063 $\pm$ 0.0009 for CMX-5A and 1.0158 $\pm$ 0.0232 for CMX-5B.[26,27] It has also been reported that the CMX-5B pellet had a more heterogeneous isotopic composition than CMX-5A.[20,26,27] Several of the CMX-5A particles analyzed in this study gave PSA ratio values centered around the target enrichment value ($^{235}U/^{238}U$ = 0.01); however, it is evident that there is a wide range of enrichment values across the 15 individual particles analyzed ($^{235}U/^{238}U \approx 0.006–0.033$). This is also the case for the CMX-5B particles, which had PSA $^{235}U/^{238}U$ atom ratios ranging from ~0.0025 to 0.0470.

DOI: 10.1021/acsomega.9b02703
ACS Omega 2020, 5, 296–303

However, unlike CMX-5A, the mean PSA $^{235}U/^{238}U$ determined by NanoSIMS for the CMX-5B particles was significantly different from the value quoted by the CEA. Here, the majority of the CMX-5B particles had a depleted ^{235}U content, yet the mean PSA for all particles is raised by the presence of a single LEU particle with an outlying $^{235}U/^{238}U$ atom ratio of 0.0473 ± 0.0001.

Detailed nanoscale imaging was obtained for all particles. Two particles from CMX-5A (CMX-5A-8 and CMX-5A-15) and two from CMX-5B (CMX-5A-10 and CMX-5A-18) were selected for presentation herein (as denoted by arrows in Figure 1). These particles were chosen as they were either deemed representative of the dataset, were measured with different isotopic pairs, or, in the example of CMX-5A-18, represented an extreme outlier.

2.3.1. CMX-5A. NanoSIMS imaging revealed an inhomogeneous $^{235}U/^{238}U$ distribution at a micrometer scale within individual CMX-5A particles. Particle CMX-5A-8 is shown in Figure 2 and is approximately 98 μm^2 (16 μm diameter). This

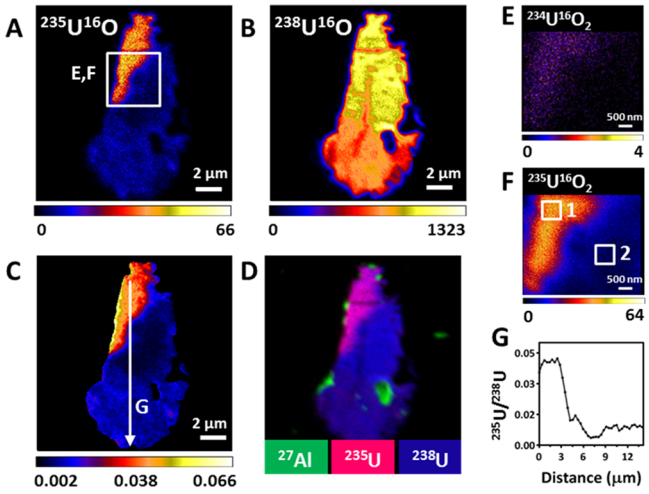

Figure 2. (A) $^{235}U^{16}O^+$ and (B) $^{238}U^{16}O^+$ secondary ion images from CMX-5A-8 in an 18 × 18 μm field of view. The values and color scale represent the count rate. (C) $^{235}U^{16}O^+/^{238}U^{16}O^+$ ratio image (with values indicated by the color scale) and (D) RGB plot for the $^{27}Al^+$, $^{235}U^{16}O^+$, and $^{238}U^{16}O^+$ across the particle. (E) $^{234}U^{16}O_2^+$ and (F) $^{235}U^{16}O_2^+$ secondary ion images from a 5 × 5 μm field of view within the main particle and two ROIs shown within the image. The locations of panels (E) and (F) are indicated by a white box in panel (A). (G) Line profile from the ratio image. The ratio images were smoothed to match the beam diameter, which was ∼300 nm.

particle exhibited a $^{235}U/^{238}U$ PSA of 0.01346 (± 0.00003) although it is evident from the $^{235}U^{16}O^+$ and $^{238}U^{16}O^+$ secondary ion images (Figure 2A,B) that there is an inhomogeneous distribution of these isotopes. Three discrete areas of ^{235}U enrichment can be discerned from the ratio image map (Figure 2C). A broad area (∼8 μm in length) of relatively high enrichment ($^{235}U/^{238}U \approx 0.040$) is located toward the top of the particle, with a well-defined boundary, directly neighboring a region of DU ($^{235}U/^{238}U \approx 0.003$). Both values correspond well to the specified enrichments of the two starting materials, suggesting incomplete mixing in broad regions (micrometer scale) of the fuel pellet. A third group of values, comprising the largest area within the particle by pixel frequency (Figure 2C), gave a range of enrichments closer to the target value ($^{235}U/^{238}U$ = 0.01). The variation in enrichment values across the length of the particle is shown as a line profile (14 × 0.7 μm) in Figure 2G, giving the $^{235}U/^{238}U$ ratio in 350 nm steps (for an approximately 300 nm beam). This particle contained a number of Al inclusions, also observed with SEM−EDX and depicted in the RGB image in Figure 2D; however, no spatial correlations could be found between these signals and the variability in the U isotopic ratios.

A 5 × 5 μm analysis window (Figure 2E,F) was also used to examine the $^{235}U/^{238}U$ ratio over the boundary region of incomplete mixing, denoted by the box in Figure 2A. The $^{235}U/^{238}U$ ratios were 0.0422 ± 0.0002 and 0.0044 ± 0.0001 for ROIs 1 and 2, respectively. $^{234}U^+$ was also analyzed in this region (as $^{234}U^{16}O_2^+$), displaying a heterogeneous spatial distribution consistent with ^{235}U enrichment; that is, heightened $^{234}U^+$ signals are associated with heightened $^{235}U^+$ signals. This is to be expected as light U isotopes are often separated together during enrichment processes.[28] The $^{234}U/^{238}U$ atom ratio ranged from 0.000357 ± 0.000023 in the enriched area (Figure 2F, ROI 1) to 0.000019 ± 0.000005 in the depleted area (Figure 2F, ROI 2). Isotopic analysis performed by the other participating laboratories showed the $^{234}U/^{238}U$ atom ratio for the CMX-5A pellet to range from ∼0.000072 to 0.000105, with the corresponding $^{235}U/^{238}U$ ratio ranging from ∼0.00980 to 0.01050.[20]

Isotopic images from CMX-5A-15 are shown in Figure 3. This particle is nearly 15× larger than CMX-5A-8 and is the largest

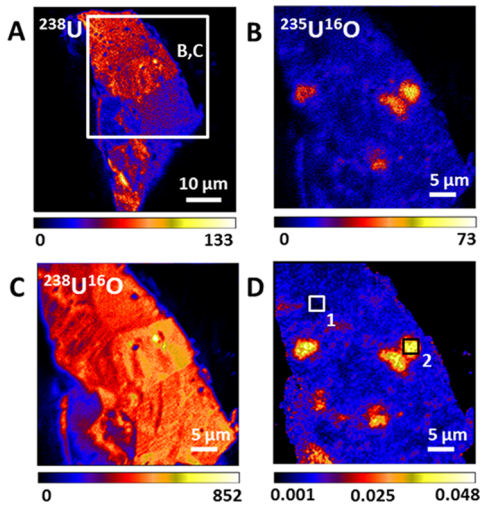

Figure 3. NanoSIMS imaging of CMX-5A-15. (A) $^{238}U^+$ image for the whole particle (62 × 62 μm field of view). A white box shows the region selected for high-resolution analysis (panels (B) and (C)). (B) Corresponding $^{235}U^{16}O^+$ image from the selected 30 × 30 μm area and (C) $^{238}U^{16}O^+$ image. The color scale and values indicate the count rate for the secondary ion images. (D) Ratio image for $^{235}U/^{238}U$, displaying two ROIs for the lowest (ROI 1) and highest (ROI 2) $^{235}U^{16}O/^{238}U^{16}O$ ratios (2.8 μm^2), with the ratio value indicated by the color scale.

CMX-5A particle analyzed (1415 μm^2), exhibiting a $^{235}U/^{238}U$ PSA of 0.0130 ± 0.0001. As with CMX-5A-8, this particle also contained discrete areas of variable ^{235}U enrichment, away from the target mixing value ($^{235}U/^{238}U$ = 0.01), with the greatest $^{235}U/^{238}U$ atom ratio being 0.0352 ± 0.0005 (ROI 2, Figure 3D). Here, the enriched areas are present as small (∼0.5 to 4 μm diameter) subspherical inclusions, sporadically dispersed throughout the particle. Regions with a depleted $^{235}U/^{238}U$

DOI: 10.1021/acsomega.9b02703
ACS Omega 2020, 5, 296−303

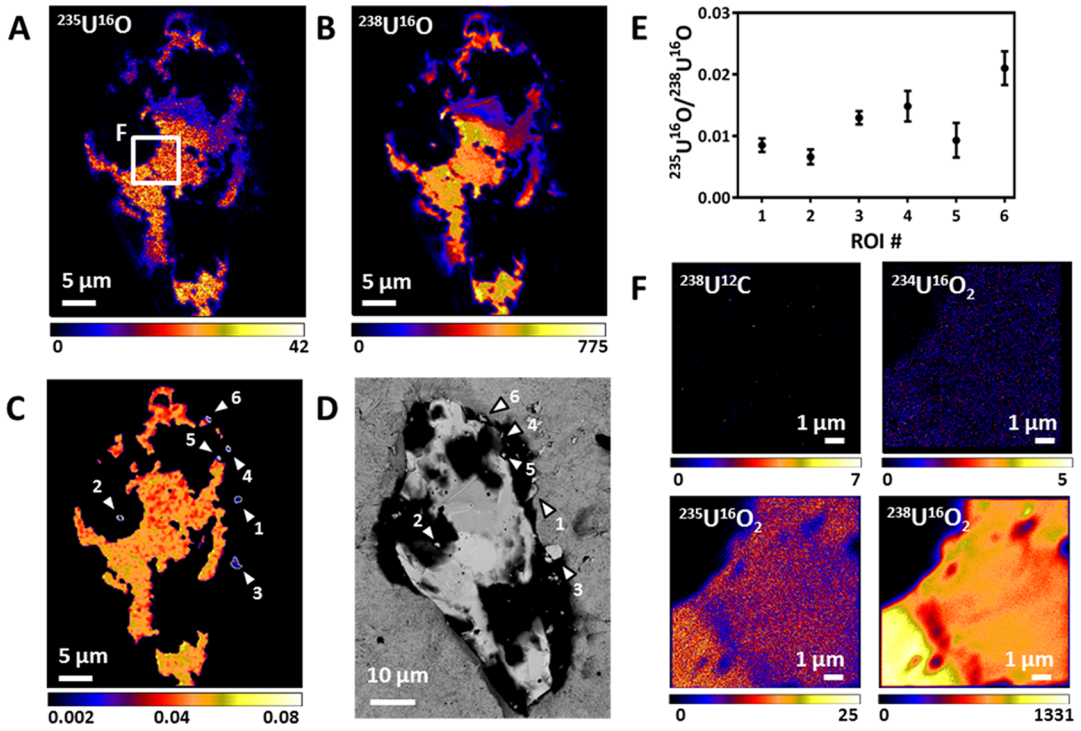

Figure 4. (A) $^{235}U^{16}O^+$ and (B) $^{238}U^{16}O^+$ secondary ion signals from CMX-5B-18. (C) $^{235}U^{16}O^+/^{238}U^{16}O^+$ ratio image indicating a central LEU particle (~4% ^{235}U) and six discrete submicrometer particles with ~1% ^{235}U. (D) Corresponding SEM (BSE) image with these six particles marked. (E) $^{235}U^{16}O^+/^{238}U^{16}O^+$ ratios for the ROIs shown in panels (C) and (D). (F) $^{238}U^{12}C^+$, $^{234}U^{16}O_2^+$, $^{235}U^{16}O_2^+$, and $^{238}U^{16}O_2^+$ secondary ion images from a 15 × 15 μm field of view, indicated by the white box in panel (A).

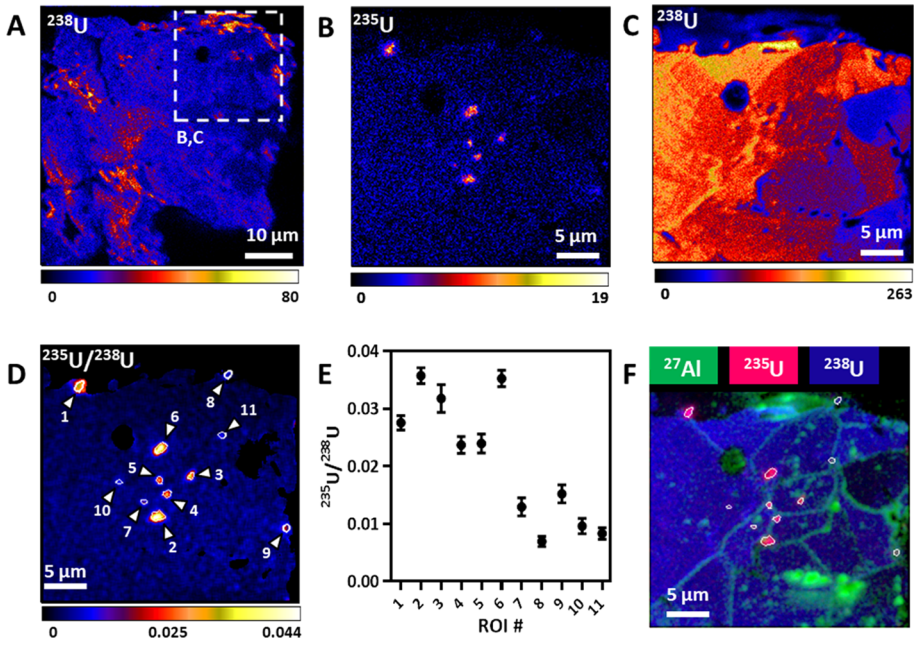

Figure 5. (A) $^{238}U^+$ signal from the entire CMX-5B-10 particle, with a white dashed box indicating a 30 × 30 μm area containing heterogeneous U isotope distribution. (B) $^{235}U^+$ and (C) $^{238}U^+$ secondary ion images from within the 30 × 30 μm region of interest. (D) Ratio image of $^{235}U/^{238}U$ with labelled ROIs. (E) Corresponding ratio values for these ROIs. (F) RGB map for $^{27}Al^+$, $^{235}U^+$, and $^{238}U^+$.

atom ratio were also observed, but unlike the particle shown in Figure 2 (CMX-5A-8), these ratios did not correlate with the depleted source material. Indeed, the lowest $^{235}U/^{238}U$ ratio was 0.0042 ± 0.0002, taken from ROI 1 in Figure 3D.

2.3.2. CMX-5B. The target enrichment value for CMX-5B was $^{235}U/^{238}U$ = 0.01. In this study, only 1 CMX-5B particle out of the analyzed 20 displayed a $^{235}U/^{238}U$ PSA atom ratio above 0.008. This particle, CMX-5B-18, is shown in Figure 4 (~567 μm^2) and has a $^{235}U/^{238}U$ atom ratio of 0.0473 ± 0.0001. The ratio image reveals heterogeneity in the $^{235}U/^{238}U$ ratio across the central region of the particle, ranging from ~0.040 to 0.055 (Figure 4C). However, the variability in U isotope ratios is less pronounced than within the CMX-5A samples (~0.003 to

DOI: 10.1021/acsomega.9b02703
ACS Omega 2020, 5, 296−303

0.040). Indeed, there is no evidence within this large particle for broad regions matching the expected DU source value (~0.3% ^{235}U). This particle may therefore be representative of the LEU starting material for the pellets, prior to mixing with DU. According to the CEA, the LEU source material used in the fuel pellets was itself created by mixing two discrete sources: one containing 4.2% ^{235}U ($^{235}U/U = 0.045$) at 67 wt % and another containing 4.5% ^{235}U ($^{235}U/U = 0.045$) at 33 wt %.[20] This variability in the isotopics of the source material could partly explain the inhomogeneity in the $^{235}U/^{238}U$ ratio across the main particle analyzed here; however, this does not account for the increased enrichment values of $^{235}U/^{238}U \approx 0.055$.

The $^{234}U/^{238}U$ and $^{235}U/^{238}U$ atom ratios were also measured across a 10 × 10 μm area of the large particle using the UO_2^+ signals, giving PSAs of 3.38×10^{-4} ($\pm 3.00 \times 10^{-6}$) and 0.0540 ($\pm$ 0.0001), respectively (Figure 4F). Interestingly, this $^{234}U/^{238}U$ ratio correlates with that measured from the LEU region within the CMX-5A particle shown in Figure 2. However, the ^{235}U enrichment is greater than that reported by the CEA and is an unexplained anomaly. The bulk $^{234}U/^{238}U$ atom ratio for CMX-5B reported by other participants in the exercise ranged from ~0.00006 to 0.00011, and the $^{235}U/^{238}U$ ratio ranged from ~0.0083 to 0.0115.[20]

In addition to the large, low-enriched particle, six individual smaller particles were also observed in this field of view, all of which displayed isotopic ratios close to the target for the pellet of 0.01 $^{235}U/^{238}U$ (Figure 4D,E). These fragments are wholly separate from the main particle and are also observable in the SEM image, highlighted by arrows in Figure 4C,D, with the ratios for the different ROIs given in Figure 4E.

Particle CMX-5B-10 (2956 μm^2) is shown in Figure 5 and has a PSA $^{235}U/^{238}U$ atom ratio of 0.0041 ($\pm$ 0.0001). As with the prior examples, the presence of submicrometer-sized areas with elevated $^{235}U/^{238}U$ ratios is evidence for incomplete mixing of the source materials. A high-resolution analysis over a 30 μm^2 field of view shows that a range of ^{235}U enrichments exists between these discrete areas, spanning from 0.0083 ($\pm$ 0.0010) to 0.0357 ($\pm$ 0.0014) (Figure 5D,E).

Interestingly, an elevated $^{27}Al^+$ signal is distributed along individual grain boundaries within this particle (Figure 5F). Further, small (<1 μm) areas enriched in ^{235}U appear to lie either along these grain boundaries or at triple junctions between grains. However, since this is the only particle where this was observed, it is difficult to assess any trends between Al and U isotope distribution.

In this study, particles from the CMX-5B pellets were shown to be more isotopically heterogeneous than those from CMX-5A. Upon conclusion of the exercise, the CEA revealed that the feedstocks used to create the CMX-5B pellets were kept separate during the initial compaction before being recombined in a soft mix. It is therefore likely that the two source materials used for the CMX-5B pellets were not homogeneously dispersed before final compaction and sintering.

The mean $^{235}U/^{238}U$ PSAs for all CMX-5B particles (0.0063 $\pm$ 0.0094) was significantly different from that described by the target manufacturer (~0.01). Of the 20 particles analyzed, 90% had a PSA in the DU range, while just 2% matched the LEU source. LG-SIMS results from another laboratory participating in the exercise also found two discrete groups of particles from the CMX-5B pellet from a larger sample set (~1000 particles), with ~90% being DU and ~10% being LEU, giving an overall enrichment of ~1% ^{235}U.[20] Here, the limited sample set of 20 particles may not reflect the average enrichment of the whole CMX-5B pellet; however, it is evident that the isotopic variation at the micrometer scale contains information on the source materials used in the pellet fabrication. NanoSIMS is the only technique that has been able to spatially resolve and image these constituent source materials on a sub-micrometer scale within individual particles.

SIMS techniques were used by several of the CMX-5 participant laboratories to characterize the two fuel pellet types.[20] The results presented from these different techniques were in broad agreement with the isotopic information released by the CEA, with average isotopic ratios representative of the target $^{235}U/^{238}U = 0.01$. The high throughput of LG-SIMS makes this technique complementary to NanoSIMS, especially in the examination of data biasing from a small sample set. There is also the potential to analyze a greater number of particles with NanoSIMS by employing automated screening software (i.e., CAMECA Automated Particle Measurement Software), but this was not available for this study.

3. CONCLUSIONS

This work highlights the suitability of the NanoSIMS 50L for nuclear forensic investigations, particularly in the determination of variable U isotopic ratios within individual, micrometer scale particles. Particles from both the CMX-5A and CMX-5B exercise materials were shown to contain inhomogeneous $^{235}U/^{238}U$ ratios on a sub-micrometer scale using a NanoSIMS 50L, allowing novel insights into the sources and processing histories of the individual fuel pellets to be obtained.

It is difficult to compare the isotopic information determined by NanoSIMS measurements with those gained from complete destructive analysis (i.e., the consumption of a whole particle performed with LG-SIMS) as NanoSIMS is a surface probe technique. This means that only a few atomic layers of material are removed during a NanoSIMS imaging analysis[23] and, as the isotopic and chemical composition of a particle may change with depth, the bulk ratio of the particle may be different to that observed at the surface. However, conventional SIMS methods that require a large primary ion beam size (i.e., greater than that of the particle) or more traditional radiochemical techniques (i.e., spectrometry, wet chemical methods) are not capable of discerning subtle isotopic and elemental disparities within an individual particle. Furthermore, this study has demonstrated that by averaging the isotopic ratios across individual particles, detailed information on the initial source materials is lost due to the scale of analysis. NanoSIMS 50L provides a means of analyzing U oxide fuel characteristics at the single particle level, making it a valuable asset in the nuclear forensic toolkit.

4. EXPERIMENTAL METHODS

4.1. Sample Preparation for NanoSIMS. Particles from each fuel pellet (CMX-5A and CMX-5B) were transferred onto separate filter paper swipes. Individual particles were then removed from the filter paper using ultrafine point tweezers under an optical microscope. These were transferred onto clean glass slides before being pressed into indium foil (99.99% purity, Sigma-Aldrich 357,294) using a vice press. The indium sections were secured onto 10 mm aluminum mounts using Torr Seal low vapor pressure epoxy.

Calibration materials were embedded in Araldite 502 epoxy resin in 10 mm diameter embedding rings made from a Ni−Cu alloy. Resin-embedded samples were ground with sequentially increasing grades of SiC grinding paper (800−2000 grit) and

DOI: 10.1021/acsomega.9b02703
ACS Omega 2020, 5, 296−303

then polished using alumina suspensions (6, 3, 1, and 0.1 μm) (Ted Pella, Inc., USA). All samples were Pt-coated (10 nm) and stored in polypropylene containers inside a desiccator cabinet prior to analysis. Trace element mass positions and secondary ion yields were calibrated using metallic Al, Fe, Cu, and Cr; Mg as $MgSO_4$; and Si from a silicon wafer. These materials were contained within a single holder. A second holder contained a natural U mineral (uranophane), and a third contained a Certified Reference Material (CRM U630, New Brunswick Laboratory, USA).[25] Radioactive materials were handled with guidance from The University of Manchester Radiation Safety Unit.

4.2. NanoSIMS 50L. SIMS analyses were completed with a NanoSIMS 50L (CAMECA, France) at The University of Manchester over three analysis sessions. The first session was performed using a duoplasmatron, which was subsequently replaced with a Hyperion II (H201) radio frequency plasma source (Oregon Physics, USA) for the remaining sessions. Details on the differences in spatial resolution between the two primary ion sources can be found in the Supporting Information (section 4, Figure S5). A 16 keV O^- primary ion beam with a current of 4.4−17.8 pA for the Hyperion II and 10.1−19.3 pA for the duoplasmatron was used to generate positive secondary ion images. Presputtering/implantation with a high current beam was used at a dose of $\sim 1.4 \times 10^{-17}$ ions/cm^2 prior to analysis in order to remove the Pt coating and increase the secondary ion yield. The multicollection detector array on the NanoSIMS 50L permits the simultaneous detection of seven ionic species. Six of the detectors are mobile, and the seventh is in a fixed position. The detectors were aligned and optimized for the chosen masses, which were varied for the different experimental sessions (see the Supporting Information, section 5). The NanoSIMS 50L allows the simultaneous multicollection of masses with one unit mass spacing up to m/z 58; thus, $^{235}U^+$ and $^{238}U^+$ must be analyzed using alternating magnetic fields, or peak-switching, with collection on a single detector. Several acquisitions also included the simultaneous detection of $^{234}U^+$ with $^{238}U^+$, which was achieved by placing the $^{234}U^+$ on a different detector. Details of the various detector alignments and beam parameters are specified in the Supporting Information (section 5, Table S2). A dwell time of 5000 μs/pixel was used for $^{235}U^+$, and 2000 μs/pixel was used for all other masses. When $^{234}U^+$ was included, a dwell time of 5000 μs/pixel was used across all detectors. All images were taken with a pixel resolution of 256 × 256 pixels, and the entrance and aperture slits were kept at 20 (ES-3) and 150 μm (AS-2), respectively. A minimum of five image planes were acquired for each particle, but the total number of image planes varied depending on the particle size and count rate. Images were dead-time-corrected (44 ns), summed, and lateral-drift-corrected. This data was processed offline using L'IMAGE software (Larry Nittler, Carnegie Institute, USA),[29] and ratio errors were calculated using a Poisson distribution of the secondary ions. Secondary ion images are presented as color maps with an arbitrary intensity scale, which is different for each ion species. Ratio images were generated by pixel smoothing using a width representative of the beam size (Table S2).

4.3. Scanning Electron Microscopy−Energy-Dispersive X-ray Spectroscopy. The SEM images were collected using an FEI Quanta 650 at 10 keV. Images were coupled with EDX to identify and map the elemental composition across individual CMX-5 particles. These samples were prepared using the method described for NanoSIMS sample preparation or by pressing particles on to an adhesive carbon pad (10 mm) on a 12 mm aluminum stub.

■ ASSOCIATED CONTENT

Supporting Information

The Supporting Information is available free of charge at https://pubs.acs.org/doi/10.1021/acsomega.9b02703.

SEM−EDX images, a porosity assessment of CMX-5A and CMX-5B particles, information on the measurement of uranium hydride interferences, a comparison of the primary ion beams used on NanoSIMS, and the NanoSIMS analysis parameters for each particle measurement (PDF).

■ AUTHOR INFORMATION

Corresponding Authors

*E-mail: connaugh.fallon@postgrad.manchester.ac.uk (C.M.F.).

*E-mail: gareth.law@helsinki.fi (G.T.W.L).

ORCID

Connaugh M. Fallon: 0000-0001-9482-3443

William R. Bower: 0000-0003-2070-2483

Gareth T. W. Law: 0000-0002-2320-6330

Notes

The authors declare no competing financial interest.

■ ACKNOWLEDGMENTS

The University of Manchester NanoSIMS was funded by UK Research Partnership Investment Fund (UKRPIF) Manchester RPIF Round 2. This work was also supported by a PhD bursary to CMF from AWE and the UK EPSRC Next Generation Nuclear Centre for Doctoral Training (EP/L015390/1), the Henry Royce Institute for Advanced Materials (funded through EPSRC grants EP/R00661X/1, EP/S019367/1, EP/P025021/1, and EP/P025498/1), and UK NERC grant NE/M014088/1 (GTWL, ICL, FRL, and WRB). We also thank Katie Moore and Greg McMahon for their technical assistance and advice, and The University of Manchester Radiation Safety Unit for guidance.

■ REFERENCES

(1) Keegan, E.; Kristo, M. J.; Toole, K.; Kips, R.; Young, E. Nuclear Forensics: Scientific Analysis Supporting Law Enforcement and Nuclear Security Investigations. *Anal. Chem.* **2016**, *88*, 1496−1505.

(2) Mayer, K.; Wallenius, M.; Ray, I. Nuclear Forensics—a Methodology Providing Clues on the Origin of Illicitly Trafficked Nuclear Materials. *Analyst* **2005**, *130*, 433−441.

(3) Mayer, K.; Wallenius, M.; Lützenkirchen, K.; Galy, J.; Varga, Z.; Erdmann, N.; Buda, R.; Kratz, J.-V.; Trautmann, N.; Fifield, K. Nuclear Forensics: A Methodology Applicable to Nuclear Security and to Non-Proliferation. *J. Phys. Conf. Ser.* **2011**, *312*, No. 062003.

(4) International Atomic Energy Agency. *Nuclear Forensics Support*; International Atomic Energy Agency: Vienna, 2006; pp 1−81.

(5) Crean, D. E.; Corkhill, C. L.; Nicholls, T.; Tappero, R.; Collins, J. M.; Hyatt, N. C. Expanding the Nuclear Forensic Toolkit: Chemical Profiling of Uranium Ore Concentrate Particles by Synchrotron X-Ray Microanalysis. *RSC Adv.* **2015**, *5*, 87908−87918.

(6) International Atomic Energy Agency. *Radioactive Particles in the Environment: Sources, Particle Characterization and Analytical Techniques*; International Atomic Energy Agency: Vienna, 2011; pp 1−90.

(7) Walther, C.; Denecke, M. A. Actinide Colloids and Particles of Environmental Concern. *Chem. Rev.* **2013**, *113*, 995−1015.

DOI: 10.1021/acsomega.9b02703
ACS Omega 2020, 5, 296−303

(8) Zendel, M.; Donohue, D. L.; Kuhn, E.; Deron, S.; Biro, T. Nuclear Safeguards Verification Measurement Techniques. In *Handbook of Nuclear Chemistry*; Vértes, A., Nagy, S., Klencsár, Z., Lovas, R. G., Rösch, F., Eds.; Springer US: Boston, 2011; pp 2896−3015, DOI: 10.1007/978-1-4419-0720-2.
(9) Mayer, K.; Wallenius, M.; Varga, Z. Nuclear Forensic Science: Correlating Measurable Material Parameters to the History of Nuclear Material. *Chem. Rev.* **2013**, *113*, 884−900.
(10) Betti, M. Isotope Ratio Measurements by Secondary Ion Mass Spectrometry (SIMS) and Glow Discharge Mass Spectrometry (GDMS). *Int. J. Mass Spectrom.* **2005**, *242*, 169−182.
(11) Betti, M.; Tamborini, G.; Koch, L. Use of Secondary Ion Mass Spectrometry in Nuclear Forensic Analysis for the Characterization of Plutonium and Highly Enriched Uranium Particles. *Anal. Chem.* **1999**, *71*, 2616−2622.
(12) Fauré, A.-L.; Dalger, T. Age Dating of Individual Micrometer-Sized Uranium Particles by Secondary Ion Mass Spectrometry: An Additional Fingerprint for Nuclear Safeguards Purposes. *Anal. Chem.* **2017**, *89*, 6663−6669.
(13) Boulyga, S.; Konegger-Kappel, S.; Richter, S.; Sangély, L. Mass Spectrometric Analysis for Nuclear Safeguards. *J. Anal. At. Spectrom.* **2015**, *30*, 1469−1489.
(14) Malherbe, J.; Penen, F.; Isaure, M. P.; Frank, J.; Hause, G.; Dobritzsch, D.; Gontier, E.; Horréard, F.; Hillion, F.; Schaumlöffel, D. A New Radio Frequency Plasma Oxygen Primary Ion Source on Nano Secondary Ion Mass Spectrometry for Improved Lateral Resolution and Detection of Electropositive Elements at Single Cell Level. *Anal. Chem.* **2016**, *88*, 7130−7136.
(15) Kips, R.; Weber, P. K.; Kristo, M. J.; Jacobsen, B.; Ramon, E. C. Microscale Isotopic Variation in Uranium Fuel Pellets with Implications for Nuclear Forensics. *Anal. Chem.* **2019**, 11598.
(16) Pajo, L.; Tamborini, G.; Rasmussen, G.; Mayer, K.; Koch, L. A Novel Isotope Analysis of Oxygen in Uranium Oxides: Comparison of Secondary Ion Mass Spectrometry, Glow Discharge Mass Spectrometry and Thermal Ionization Mass Spectrometry. *Spectrochim. Acta Part B* **2001**, *56*, 541−549.
(17) Mueller, C. W.; Weber, P. K.; Kilburn, M. R.; Hoeschen, C.; Kleber, M.; Pett-Ridge, J. Advances in the Analysis of Biogeochemical Interfaces: NanoSIMS to Investigate Soil Microenvironments. *Adv. Agron.* **2013**, *121*, 1−46.
(18) Schwantes, J. M.; Marsden, O.; Pellegrini, K. L. State of Practice and Emerging Application of Analytical Techniques of Nuclear Forensic Analysis: Highlights from the 4th Collaborative Materials Exercise of the Nuclear Forensics International Technical Working Group (ITWG). *J. Radioanal. Nucl. Chem.* **2017**, *311*, 1441−1452.
(19) Garrett, B. C.; Mayer, K.; Thompson, P.; Pong, B. K.; Lasou, G.; K Pong, B.; Lasou, G. The Nuclear Forensics International Technical Working Group (ITWG) An Overview. In *International Conference on Advances in Nuclear Forensics: Countering the Evolving Threat of Nuclear and Other Radioactive Material out of Regulatory Control*; International Atomic Energy Agency: Vienna, Austria, 2014; pp 1−8.
(20) Schwantes, J. M.; Marsden, O.; Taylor, F. *ITWG 5th Collaborative Materials Exercise After Action Report*; unpublished work.
(21) Parsons-Davis, T.; Knight, K.; Fitzgerald, M.; Stone, G.; Caldeira, L.; Ramon, C.; Kristo, M. Application of Modern Autoradiography to Nuclear Forensic Analysis. *Forensic Sci. Int.* **2018**, *286*, 223−232.
(22) International Atomic Energy Agency. *Fuel Performance at High Burnup for Water Reactors*; International Atomic Energy Agency: Vienna, Austria, 1991, ISSN 1011−2766.
(23) Kilburn, M. R.; Wacey, D. Nanoscale Secondary Ion Mass Spectrometry (NanoSIMS) as an Analytical Tool in the Geosciences. In *Principles and Practice of Analytical Techniques in Geosciences*; Grice, K., Ed.; The Royal Society of Chemistry: Cambridge, 2015; pp 1−34, DOI: 10.1039/9781782625025-00001.
(24) Simons, D. S.; Fassett, J. D. Measurement of Uranium-236 in Particles by Secondary Ion Mass Spectrometry. *J. Anal. At. Spectrom.* **2017**, *32*, 393−401.
(25) New Brunswick Laboratory. *Certificate of Analysis: CRM U630*; New Brunswick Laboratory: 2013.
(26) Girard, P. Manufacturing and Characterizations of Two Batches of UO_2 Pellets for ITWG/ CMX-5. In *CMX-5 Data Review Meeting*; Bucharest, Romania, 2017. As cited in Krachler *et al.*, (2019).
(27) Krachler, M.; Varga, Z.; Nicholl, A.; Wallenius, M.; Mayer, K. Spatial Distribution of Uranium Isotopes in Solid Nuclear Materials Using Laser Ablation Multi-Collector ICP-MS. *Microchem. J.* **2018**, *140*, 24−30.
(28) Tam Nguyen, C. Age-Dating of Highly Enriched Uranium by γ-Spectrometry. *Nucl. Instr. Meth. Phys. Res. B* **2005**, *229*, 103−110.
(29) Nittler, L. *L'Image (IDL-120618)*; Carnegie Institution of Washington: Washington, DC, 2019.

DOI: 10.1021/acsomega.9b02703
ACS Omega 2020, 5, 296−303